The Climatic Importance of Uncertainties in Regional Aerosol–Cloud Radiative Forcings over Recent Decades

LEIGHTON A. REGAYRE, KIRSTY J. PRINGLE, LINDSAY A. LEE, ALEXANDRU RAP, JO BROWSE, GRAHAM W. MANN,* CARLY L. REDDINGTON, AND KEN S. CARSLAW

Institute for Climate and Atmospheric Science, School of Earth and Environment, University of Leeds, Leeds, United Kingdom

BEN B. B. BOOTH

Met Office Hadley Centre for Climate Change, Exeter, United Kingdom

MATTHEW T. WOODHOUSE

CSIRO Oceans and Atmosphere, Aspendale, Victoria, Australia

(Manuscript received 10 February 2015, in final form 1 May 2015)

ABSTRACT

Regional patterns of aerosol radiative forcing are important for understanding climate change on decadal time scales. Uncertainty in aerosol forcing is likely to vary regionally and seasonally because of the short aerosol lifetime and heterogeneous emissions. Here the sensitivity of regional aerosol cloud albedo effect (CAE) forcing to 31 aerosol process parameters and emission fluxes is quantified between 1978 and 2008. The effects of parametric uncertainties on calculations of the balance of incoming and outgoing radiation are found to be spatially and temporally dependent. Regional uncertainty contributions of opposite sign cancel in global-mean forcing calculations, masking the regional importance of some parameters. Parameters that contribute little to uncertainty in Earth's global energy balance during recent decades make significant contributions to regional forcing variance. Aerosol forcing sensitivities are quantified within 11 climatically important regions, where surface temperatures are thought to influence large-scale climate effects. Substantial simulated uncertainty in CAE forcing in the eastern Pacific leaves open the possibility that apparent shifts in the mean ENSO state may result from a forced aerosol signal on multidecadal time scales. A likely negative aerosol CAE forcing in the tropical North Atlantic calls into question the relationship between Northern Hemisphere aerosol emission reductions and CAE forcing of sea surface temperatures in the main Atlantic hurricane development region on decadal time scales. Simulated CAE forcing uncertainty is large in the North Pacific, suggesting that the role of the CAE in altering Pacific tropical storm frequency and intensity is also highly uncertain.

1. Introduction

Aerosols affect Earth's climate by absorbing and scattering solar and terrestrial radiation (Twomey 1977; Boucher et al. 2013). The cloud albedo effect (CAE) (Boucher et al. 2013), characterized by a decrease in cloud drop effective radius that results from an increase in cloud droplet number concentration for a given amount of liquid water (Twomey 1977), is the largest component of the aerosol–cloud interaction. Uncertainty in the magnitude of CAE forcing remains the dominant source of uncertainty in net aerosol radiative forcing within current global climate models (Skeie et al. 2011; IPCC 2013).

Anthropogenic aerosol emission fluxes and aerosol process parameters were identified by Regayre et al. (2014) as the largest sources of simulated global-mean

Denotes Open Access content.

* Current affiliation: National Centre for Atmospheric Science, University of Leeds, Leeds, United Kingdom.

Corresponding author address: Leighton A. Regayre, Institute for Climate and Atmospheric Science, School of Earth and Environment, University of Leeds, Leeds, LS2 9JT, United Kingdom.
E-mail: laregayre11@leeds.ac.uk

DOI: 10.1175/JCLI-D-15-0127.1

CAE forcing variance in recent decades; however, credible ranges of global-mean CAE forcing were found to be small compared to the magnitude of forcing resulting from changes in atmospheric CO_2 concentrations. Regayre et al. (2014) hypothesized that a large component of multimodel CAE forcing diversity during recent decades is determined by the extent to which regional positive and negative forcings cancel in individual models when calculating global-mean CAE forcing.

The magnitude of large-scale climatic responses, such as global-mean surface temperature, are sensitive to the spatial position of regional forcings (Shindell et al. 2013), making it important to understand CAE forcing at the regional scale. In this paper we aim to identify the aerosol process parameters and emission fluxes, hereafter referred to as parameters, which are the largest sources of regional-mean CAE forcing variance and also have potential to be influential on global-mean forcing in near-future climates.

We compare the Regayre et al. (2014) global-mean CAE forcing results with an analysis that accounts for cancellation of positive and negative regional forcings. The CAE forcing sensitivity to the 31 aerosol parameters is quantified within 11 regions where CAE forcing potentially influences large-scale climate effects such as monsoon intensity, tropical storm development, and precipitation. The statistical analyses conducted here highlight aspects of aerosol research and model development that should be prioritized in order to reduce the impact of uncertainty in regional CAE forcings on near-term climate projections.

2. Methods

a. Perturbed parameter ensemble

The Global Model of Aerosol Processes (GLOMAP) (Spracklen et al. 2005; Mann et al. 2010, 2012) was used by Regayre et al. (2014) to create the perturbed parameter ensemble used in this research. Each ensemble member has a horizontal resolution of 2.8° × 2.8° with 31 vertical levels between the surface and 10 hPa. GLOMAP is an extension of the TOMCAT chemical transport model (Stockwell and Chipperfield 1999). To create each ensemble member, 31 aerosol process parameters and emission fluxes were perturbed simultaneously. Maximin Latin hypercube sampling was used to create a parameter combination design, of 186 points, that spans the 31-dimensional uncertain parameter space. The probability distributions for the uncertain parameters used in Regayre et al. (2014) were identified through expert elicitation updated from Lee et al. (2013). A further simulation with all parameters set to their median values was included in the ensemble to ensure coverage of what experts believed to be an important region of parameter space.

In the version of the GLOMAP model used to create the ensemble, three-dimensional meteorological fields and cloud distributions for all years were obtained from the European Centre for Medium-Range Weather Forecasts (ECMWF) interim reanalysis (ERA-Interim) for 2008. Low-level stratiform clouds were prescribed from the International Satellite Cloud Climatology Project (ISCCP) D2 data (Rossow and Schiffer 1999). Modeled aerosols are affected by cloud processing and precipitation, although changes in modeled aerosols do not affect the meteorology, transport, or presence of cloud. Emission scenarios prepared for the Atmospheric Chemistry and Climate Model Intercomparison Project (ACCMIP) (Lamarque et al. 2010) and prescribed in some of the experiments from phase 5 of the Coupled Model Intercomparison Project (CMIP5) (Taylor et al. 2012) were used to prescribe anthropogenic aerosol emissions in these simulations. The experimental design is such that parameter perturbations are the sole cause of changes in simulated CAE forcing for each ensemble member.

Pairs of 1-yr simulations were used to calculate monthly and annual-mean CAE forcing. Identical model configurations were used for each pair of simulations with the exception of anthropogenic aerosol emissions, which were prescribed distinctly for each year. The definition of CAE forcing used here is identical to that of Carslaw et al. (2013) and Regayre et al. (2014), where it is regarded as the difference in top-of-atmosphere net radiative fluxes between years. CAE forcing values are calculated by modifying the cloud drop effective radius r_e for low- and midlevel clouds up to 6×10^2 hPa, within the offline version of the Edwards and Slingo (1996) radiative transfer model. Because year-2000 values of surface albedo and cloud optical depths from ISCCP D2 were used, r_e was modified relative to values derived for that year, denoted here using the superscript ref:

$$r_e = r_e^{\mathrm{ref}} \left(\frac{\mathrm{CDNC}^{\mathrm{ref}}}{\mathrm{CDNC}} \right)^{1/3}, \tag{1}$$

where CDNC is the monthly mean cloud drop number concentration within each model grid box. A cloud droplet activation parameterization (Fountoukis and Nenes 2005; Barahona et al. 2010) was used to calculate CDNC for each ensemble member in each model grid box using the monthly mean aerosol distribution and composition. A fixed value of $r_e^{\mathrm{ref}} = 10\,\mu$m was used to

ensure consistency with the ISCCP retrievals. CAE forcing over the 1978–2008 period was taken as the difference between forcings for each year relative to the year 2000. Regayre et al. (2014) show that the net cloud radiative effect from the year-2000 reference simulation is in agreement with CMIP model output (Calisto et al. 2014).

b. Sensitivity analysis

A sensitivity analysis (Saltelli et al. 2000; Lee et al. 2013) of CAE forcing in each model grid box is made possible using validated Bayesian emulators (O'Hagan 2006) that are conditioned on output from the 187 perturbed parameter simulations. The emulator of each model grid box provides a statistical approximation of CAE forcing at any point in the 31-dimensional parameter space. A further emulator is constructed using global-mean absolute CAE forcing, where the absolute value of CAE forcing for each model grid box is used in the calculation of the global mean to remove the effect of canceling regional forcings of opposing sign. This approach allows us to use a single global value to quantify the importance of individual parameters, even if changes in the parameter cause positive and negative forcings that cancel in the global-mean calculation.

The Bayesian emulation approach has been successfully applied to GLOMAP model output by Lee et al. (2011, 2012, 2013), Carslaw et al. (2013), Hamilton et al. (2014), and Regayre et al. (2014). Contributions to variance from each parameter and statistical interactions between parameters can be explicitly quantified across the multidimensional response surface. This is made possible because the emulators produce output in a fraction of the time required to produce a simulation. Large samples of output can therefore be obtained and used to produce probability distributions. The extended Fourier amplitude sensitivity test (FAST) sampling method (Saltelli et al. 1999), with 10^4 emulator sample points, was used here to obtain the data for each Monte Carlo–style sensitivity analysis.

The results of the global-mean absolute CAE forcing sensitivity analyses are contrasted with the results of the global CAE forcing sensitivity analysis of Regayre et al. (2014) in section 3a. Regional sensitivity analysis results and their climatic importance are discussed in section 3b. Here the sensitivity analysis is conducted using monthly, rather than annual, mean CAE forcing to avoid cancellation of forcings of opposite sign in different months or seasons. The statistic considered most in the discussion of these results is the percentage reduction in monthly mean CAE forcing variance that could be expected if the parameter in question were known exactly. Mean regional contributions to forcing are obtained for each month by weighting contributions to CAE forcing variance within each model grid box by the proportion of total regional forcing evident within that grid box. The CAE forcing uncertainty within regions is quantified using mean 90% credible intervals (CIs) of CAE forcing. The means of the 5th and 95th percentiles within each model grid box are used to calculate mean CIs. Regional-mean forcings and CIs are calculated using only the months where CAE forcing has been identified as climatically important, as summarized in section 2d.

c. Time period

The ensemble of 187 paired perturbed parameter simulations for the period 1978–2008 used by Regayre et al. (2014) to analyze global CAE forcing uncertainty is used here to analyze regional CAE forcing uncertainty. The 1978–2008 period produces distinct regions of positive and negative CAE forcing that result from spatial heterogeneity in the long-term trends of anthropogenic emissions. In 1978, global anthropogenic sulfate emissions peaked (Lamarque et al. 2010) then decreased in Europe and North America while increasing significantly in Asia (Smith et al. 2011). Current satellite observations reveal a persistence of these regional trends in anthropogenic emissions (Mao et al. 2014), and simulations suggest that peak regional aerosol forcing from Asian anthropogenic emissions relative to the preindustrial era may not be reached for several decades (Li et al. 2014), indicating that a sensitivity analysis of 1978–2008 CAE forcing will be informative about near-future climate uncertainties. A time series of global CAE forcing relative to the year 1850, constructed using simulations where all parameters were set to their median values, is presented in Fig. 1. The global-mean CAE forcing trend plateaus in the 1980s, making the change in forcing relative to 1850 near neutral during the 1978–2008 period.

d. Large-scale climate effects

Global models initialized with prescribed SSTs based on observations show enhanced interannual predictability of regional temperatures and precipitation (Hermanson and Sutton 2010; Robson et al. 2013). Confident prediction of large-scale climate effects relies on well-simulated SST, which in turn requires the reliable simulation of the CAE. Changing anthropogenic aerosol emissions have the potential to induce aerosol-specific changes in regional atmospheric circulation and precipitation (Kirtman et al. 2013).

Large regional uncertainties in CAE forcing will strongly influence SST and thus hinder the accurate simulation of climate effects, which affect much of

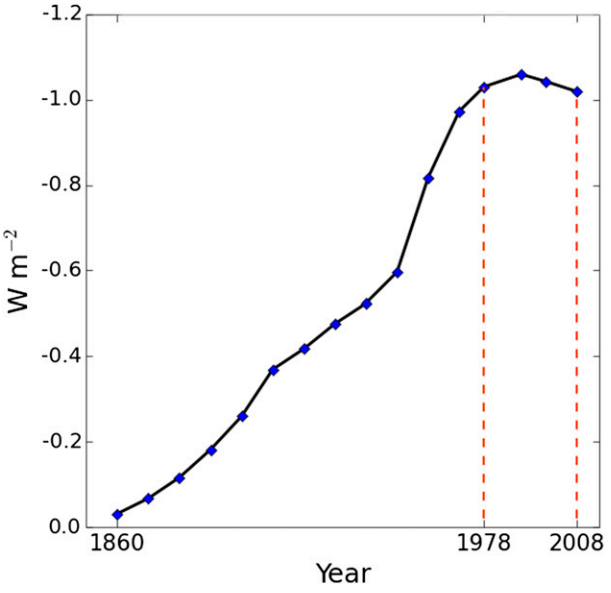

FIG. 1. Global-mean CAE forcing relative to 1850 (W m^{-2}). Simulations with all parameters in the Regayre et al. (2014) design set to their median values were used to calculate the global-mean CAE forcing values.

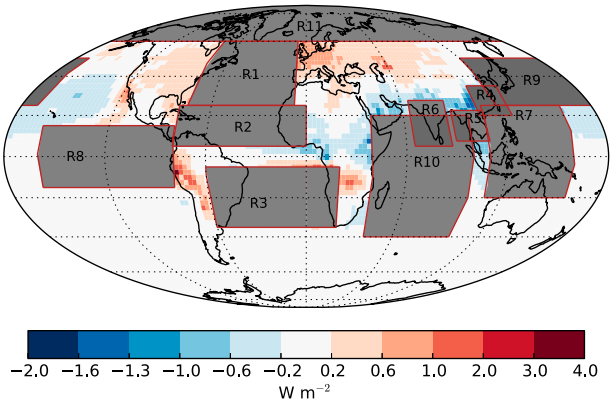

FIG. 2. Regions of climatic importance, as summarized in Table 1, overlaid onto annual-mean CAE forcing for the 1978–2008 period, taken from the simulation where all aerosol process parameters and emission fluxes are set to their median elicited values.

Earth's population. Table 1 and Fig. 2 indicate the location of the 11 regions (R1–R11) used in the regional component of this research. Regions were chosen based on the potential for changes in SST and/or surface air temperature (SAT) to influence large-scale climatic effects. The regional CAE forcing sensitivity analyses presented in section 3b are individually restricted to either marine or continental land environments. External forcings in tropical regions are more likely to induce a global temperature response than polar forcings (Roe et al. 2015). However, it is assumed that reducing uncertainty in the simulation of the climate effects outlined in this section, by reducing uncertainty in CAE forcing, will improve near-future climate projections.

1) INTERTROPICAL CONVERGENCE ZONE AND SAHEL PRECIPITATION

Ascending air near the equator is advected poleward and descends in the subtropical dry zones forming the Hadley cell. The structure of the Hadley cell determines the position of subtropical dry zones, which are important for Earth's hydrological cycle and energy balance (Seidel et al. 2008). Observational evidence suggests that the Hadley cell has widened in recent decades (Allen et al. 2012; Choi et al. 2014), which cannot be explained by greenhouse gas–induced warming (Lu et al. 2007). The width and position of the ITCZ, within which the ascending air that contributes to the Hadley cell resides, plays an important role in determining the structure of the Hadley cell (Kang and Lu 2012).

TABLE 1. Latitude and longitude ranges used to define regions where CAE forcing is known to influence SST and therefore has the potential to indirectly influence climate effects. The months indicate when SST has the greatest influence on climatic effects.

Key	Location	Lat range	Lon range	Climate effect	Relevant months
R1	Extratropical North Atlantic	25°–60°N	7°–75°W	North Atlantic tropical storms Sahel precipitation	Apr–Oct All year
R2	Tropical North Atlantic	5°–25°N	0°–80°W	North Atlantic tropical storms Atlantic ITCZ and Sahel precipitation	Apr–Oct All year
R3	Tropical South Atlantic	5°–35°S	60°W–20°E	Atlantic ITCZ and Sahel precipitation	All year
R4	East China	20°–35°N	107.5°–125°E	Asian summer monsoon	Jun–Sep
R5	Southeast Asia	7.5°–22.5°N	90°–107.5°E	Asian summer monsoon	Jun–Sep
R6	Indian subcontinent	5°–27.5°N	65°–87.5°E	Asian summer monsoon	Jun–Sep
R7	Western Pacific	20°S–25°N	107.5°–160°E	Asian summer monsoon	Jun–Sep
R8	Tropical eastern Pacific	15°S–15°N	160°–80°W	ENSO	Oct–Feb
R9	Northwestern Pacific	25°–50°N	120°E–170°W	Pacific tropical storms	Jan–Jul
R10	Indian Ocean	40°S–20°N	40°–100°E	Asian summer monsoon	Jun–Sep
R11	Arctic	60°–90°N	All lon	Arctic warming	May–Sep

The gradient in interhemispheric tropical SSTs determines the position and width of the Atlantic ITCZ (Chang et al. 2011; Cvijanovic and Chiang 2013), which affects precipitation patterns in neighboring regions (Zhang et al. 2007; Hwang et al. 2013). Anomalously cold North Atlantic SSTs relative to SSTs in the South Atlantic are correlated with a southward shift in ITCZ position and with periods of drought in the Sahel over the last century (Folland et al. 1986; Mulitza et al. 2008; Shanahan et al. 2009). A strong contrast between tropical and extratropical North Atlantic SSTs is found by Liu et al. (2014) to be an integral component of the teleconnection that allows SSTs to influence precipitation in neighboring regions. Anthropogenic aerosol emissions have prevented North Atlantic SST from warming as rapidly as South Atlantic SST in response to increasing greenhouse gas concentrations over the last century (Rotstayn and Lohmann 2002), yet since the late 1970s the gradient between Atlantic Ocean basins has declined as a result of anthropogenic aerosol emission reduction strategies in the Northern Hemisphere (Chang et al. 2011; Chiang et al. 2013; Friedman et al. 2013).

Booth et al. (2012) argue that aerosol forcing may decouple North Atlantic SSTs from Atlantic meridional overturning circulation (AMOC)-driven changes, suggesting that changing aerosol concentrations since the preindustrial period may be the dominant influence on SSTs. The relative importance of anthropogenic aerosols and the AMOC in determining North Atlantic SSTs remains unknown (Zhang et al. 2013); however, Dunstone et al. (2013, Fig. S8 in their supplementary information) revealed a correlation between the magnitude of CAE forcing in models and the degree to which CAE forcing determines Atlantic SSTs. Exploring the sources of uncertainty in CAE forcing in the Atlantic will therefore inform the possible sources of multimodel SST diversity.

2) TROPICAL STORM DEVELOPMENT REGIONS

Tropical storms have the potential to cause considerable socioeconomic damage (Pielke et al. 2008), and thus there is value in reducing uncertainty in the simulation of near-future events. Climate model simulations that make use of observed North Atlantic SSTs are capable of reproducing tropical storm frequency variance (Trenberth and Shea 2006; Zhao and Held 2012), and anthropogenic aerosols have been implicated as causing decadal changes in North Atlantic SSTs (Mann and Emanuel 2006; Evan et al. 2009; Dunstone et al. 2013). Evidence suggests that uncertainty in near-future tropical storm frequency can be reduced by improving the representation of aerosol radiative forcing within models (Villarini and Vecchi 2013).

Tropical storm development in the North Atlantic is influenced by SSTs in regions that also influence ITCZ position and Sahel precipitation as described in section 2d(1), compounding the importance of quantifying CAE forcing uncertainty in these regions. Pacific Ocean SSTs are also affected by changes in anthropogenic aerosol emissions (Boo et al. 2015), particularly from Asia (Yeh et al. 2013). The metrics used to determine the phase of the Pacific decadal oscillation and the width of the tropical storm belt contain large uncertainties that are associated with anthropogenic aerosol forcing (Allen et al. 2014). Changing atmospheric temperatures and SSTs in the northwestern Pacific in response to increasing Asian anthropogenic aerosol emissions are a likely cause of increased Pacific tropical storm frequency and intensity in recent decades, according to Wang et al. (2014a,b).

3) ASIAN SUMMER MONSOON

The Asian summer monsoon (ASM) is characterized by heavy rainfall across much of the Asian continent, providing as much as 70% of the annual rainfall to some Asian regions over the summer months (Gong and Ho 2003). The intensity of contrast between SST and continental SAT is correlated with the strength of the ASM (Webster 1987), and in recent decades a weakening of the land–sea contrast, largely attributable to anthropogenic aerosol emissions, has to a large extent counteracted the intensification of the ASM expected to result from the positive forcing associated with increasing atmospheric greenhouse gas (GHG) concentrations (Wang et al. 2013; Guo et al. 2013; Salzmann et al. 2014). Observational evidence suggests that a greater proportion of ASM precipitation occurs over southern China than in the north as a result of a weaker ASM (Ding et al. 2008; Ye et al. 2013), with flood risks and increased air pollution likely outcomes (Li et al. 2011).

Substantial anthropogenic sulfate aerosol concentrations are transported from Asian continents over the Indian Ocean during the early part of each year (Verma et al. 2013), and Fadnavis et al. (2013) established that ASM precipitation over India declines in response to anthropogenic emissions. The CAE significantly affects SST in the Indian Ocean (Yun et al. 2014), largely countering the positive CO_2 forcing in this region since the early industrial period (Dong and Zhou 2014). CAE forcing is therefore partially responsible for the early onset of the ASM resulting in heavy precipitation over the Indian subcontinent at the start of the monsoon season and reduced precipitation during the remainder of the Northern Hemisphere summer (Bollasina et al. 2013; Henriksson et al. 2014).

4) El Niño–Southern Oscillation

Aside from the seasonal cycle, the El Niño–Southern Oscillation (ENSO) is the largest mode of climate variability (Diaz et al. 2001; McPhaden et al. 2006). The El Niño phase of the ENSO results in anomalously warm SSTs in the eastern equatorial Pacific accompanying a reversal of trade winds and a slowing down of circulation within the Pacific basin (Rasmusson and Carpenter 1982).

The magnitude of aerosol forcing and its uncertainty in the region where the dominant ENSO signal manifests are considered in this paper because, although there are no established links between CAE forcing and ENSO variability, aerosols appear to project strongly onto SSTs on multidecadal time scales (Shindell et al. 2013; Regayre et al. 2014). Changes in mean SSTs interpreted as a shift toward a more El Niño or La Niña state may in fact reflect changes due to local forcing. Quantifying the uncertainty in CAE forcing in these regions will establish the potential for shifts in the ENSO mean state on decadal time scales to be a result of a forced aerosol signal.

5) Arctic

The Arctic region has experienced anomalous warming compared to the rest of Earth's surface over recent decades (Serreze et al. 2009). Much of the warming in the Arctic is attributable to the ice–albedo feedback (Screen and Simmonds 2010), where melt pools reduce the albedo of the surface, allowing for greater warming. Gillett et al. (2008) identify anthropogenic emissions as playing an essential role in warming the Arctic in recent decades. Decreasing anthropogenic aerosol concentrations transported to the Arctic from North America and Europe generate a positive CAE forcing, which has been shown to be a major cause of the observed warming (Shindell and Faluvegi 2009; Chylek et al. 2014).

e. Regional aerosol radiative forcing

The effect of each parameter perturbation on the 1978–2008 CAE forcing at each location depends on the relative changes in aerosol distributions (and hence CDNCs) in the two years. CAE forcing depends nonlinearly on CDNC changes and is more sensitive when CDNCs are low (Carslaw et al. 2013). Furthermore, the effect of aerosol parameter perturbations on forcing must be interpreted in the context of the sign of regional CAE forcing.

Six representative scenarios (S1–S6) are depicted in Fig. 3 to assist with interpreting the effect of changing CDNCs through aerosol parameter perturbations on

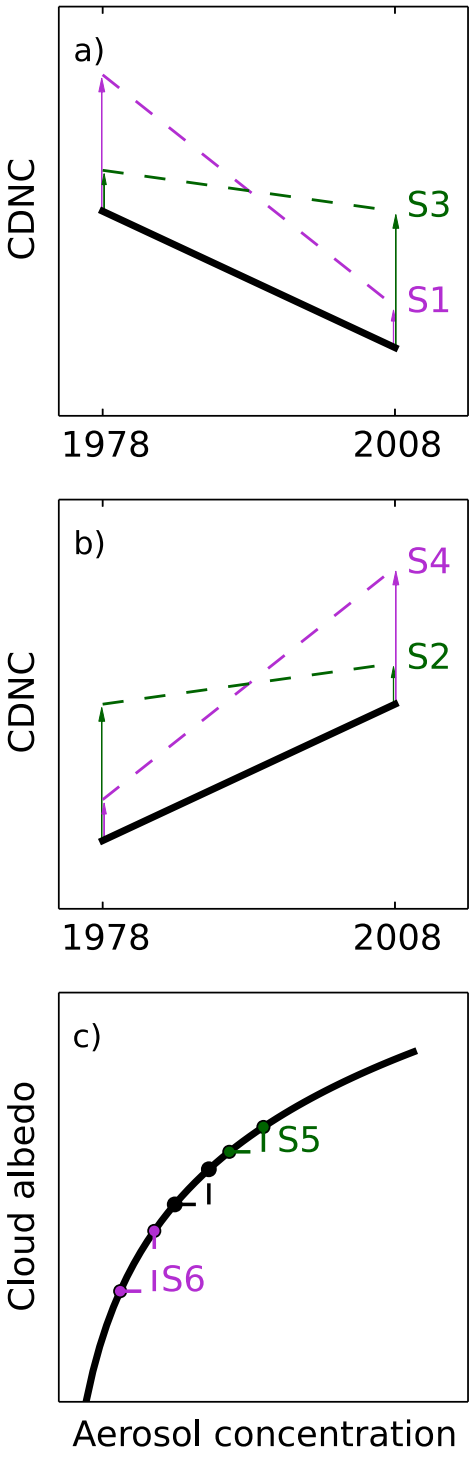

FIG. 3. Theoretical effects of perturbing parameters on (a) declining CDNC (positive CAE forcing), (b) increasing CDNC (negative CAE forcing), and (c) albedo between 1978 and 2008. Black lines represent the baseline case with no parameter perturbations. Six scenarios representing perturbed parameter cases are labeled S1–S6. Purple indicates an amplification and green indicates a suppression of CAE forcing regardless of the sign of the underlying forcing within an individual model grid box.

CAE forcing. Amplification of positive and negative CAE forcing (steeper gradient) occurs in scenarios S1 and S4, respectively, as a result of changing a parameter. In S1 the change in CDNC is largest in 1978, thereby strengthening the positive CAE forcing between 1978 and 2008 (caused by a larger net decrease in CDNC than in the baseline case). In S4 the change in CDNC is largest in 2008, thereby strengthening the negative forcing. In scenarios S2 and S3 the relative changes in CDNCs in 1978 and 2008 are identical to the changes in S1 and S4, respectively; however, the sign of forcing is reversed, and therefore in these cases the parameter perturbation causes a suppression of the CAE forcing (making the slope of the line in the perturbed case shallower than the line in the baseline case).

Absolute changes in CDNCs within a given model grid box, resulting from a parameter perturbation, may be the same in the two simulated years, but because of the nonlinear relationship between aerosol concentration and albedo (Fig. 3c) a forcing will still occur. The importance of the baseline aerosol concentration in radiative forcing calculations is discussed in Carslaw et al. (2013). A more polluted baseline is associated with a smaller temporal change in albedo; hence, scenario S5 represents a decrease in CAE forcing (relative to the baseline case) resulting from an increase in aerosol concentrations in both years. Scenario S6 represents the case where a parameter perturbation causes CDNCs in both years to decrease (relative to the baseline case), leading to a greater difference in albedo between the two years and therefore stronger CAE forcing.

Scenarios S1–S4 are all based on the assumption that CDNC increases in a region in both years as a result of the parameter perturbation. Mirror images of scenarios S1–S4 where CDNCs decrease are not shown, nor are more extreme cases where CDNCs increase in one year and decrease in the other; however, scenarios S1–S4 provide a suitable framework for examining the cancellation of regional contributions to global-mean CAE forcing variance.

3. Results

a. Global forcing sensitivities

Because contributions of opposing signs cancel, parameter perturbations that act to enhance CAE forcing in regions of both positive and negative forcing could make significant contributions to regional CAE forcing variance that are not detected in a sensitivity analysis of global-mean CAE forcing variance. Regions of substantial positive and negative forcing are evident in each of the maps in Fig. 4. Similarly, a parameter perturbation that acts to suppress CAE forcing (as described by scenarios S2 and S3) will make contributions to both positive and negative regional forcing that cancel in a global forcing calculation, whereas a parameter perturbation that acts to amplify positive regional forcings (S1) and conversely suppress negative regional forcings (S2) will not have its contribution to global-mean CAE forcing variance affected by regional forcing cancellation.

The percentage contributions to global-mean CAE forcing and global-mean absolute CAE forcing, calculated between 1978 and 2008 as described in section 2b, are compared in Fig. 5. There is no correlation evident between the global-mean forcing and global-mean absolute forcing measures. No parameter contributes more than 10% of the CAE forcing variance in both cases, suggesting that substantial cancellation of important regional contributions to global-mean CAE forcing occurs.

Contributions to CAE forcing in individual model grid boxes are presented in Fig. 6 for two parameters that contribute a substantial percentage of variance in either global-mean CAE forcing or global-mean absolute CAE forcing. The spatial pattern of CAE forcing sensitivities to parameter perturbations varies temporally, and the months displayed in Fig. 6 are representative of months where the parameters in question contribute substantially to CAE forcing variance. Only percentage contributions to variance in model grid boxes where the absolute ensemble-mean CAE forcing is greater than $0.1\,\mathrm{W\,m^{-2}}$ have been plotted (shaded purple where an increase in the value of the parameter acts to amplify CAE forcing and shaded green where forcing is suppressed, matching the shading used in Fig. 3). The spatial patterns of contributions to variance need to be analyzed in the context of the underlying spatial pattern of CAE forcing represented in Fig. 4 in order to understand the global-mean effect of perturbing a parameter.

The emission flux of organic carbon and black carbon aerosols from fossil fuel sources (FF_Ems) and the diameter of emitted particles (FF_Diam) are the largest sources of global-mean CAE forcing uncertainty (Fig. 5). Contributions to CAE forcing variance from FF_Ems for May are presented in Fig. 6a. Increasing FF_Ems typically amplifies negative CAE forcing in regions where CDNCs have increased between 1978 and 2008 (S4) yet suppresses positive CAE forcing in regions where CDNCs have declined (S3). Fossil fuel emissions are a large component of the increase in Asian CDNC, and positively perturbing FF_Ems amplifies the negative CAE forcing in this region (S4). In contrast, the positive forcing is suppressed (S3) in regions where the decrease in CDNC is not driven by carbonaceous

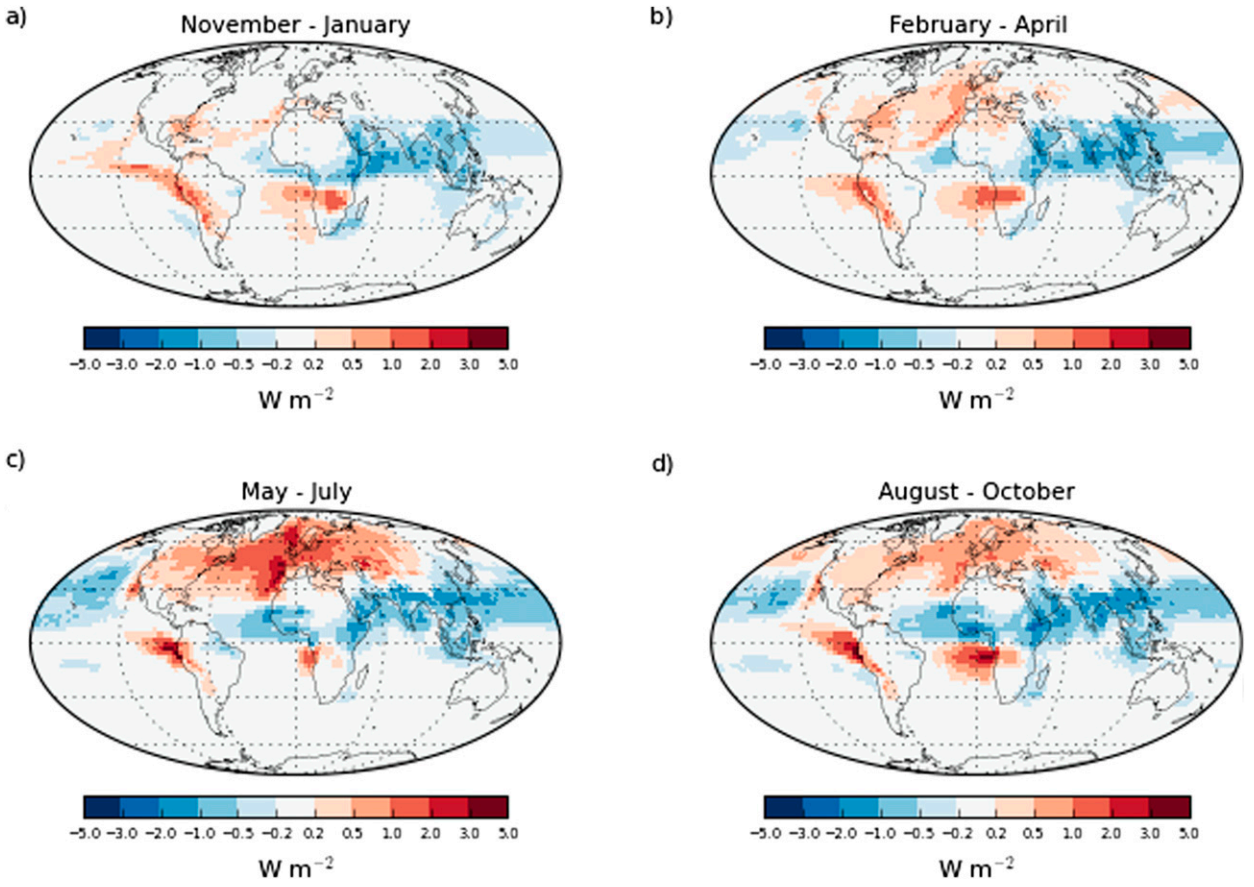

FIG. 4. Ensemble-mean CAE forcing within individual model grid boxes for (a) November–January, (b) February–April, (c) May–July, and (d) August–October during the 1978–2008 period.

aerosol emissions from fossil fuel sources (Lamarque et al. 2010; Granier et al. 2011), such as North America, because the relatively low 2008 CDNCs are more sensitive to positive FF_Ems perturbations than the higher 1978 CDNCs (S5).

Perturbing FF_Ems produces a shift in CAE forcing in the same direction for both positive and negative forcing regions. Therefore, when forcing is amplified (suppressed) in a positive forcing region, it is suppressed (amplified) in a region of negative forcing. Increasing FF_Diam produces an inverse pattern of forcing response to increasing FF_Ems because increases in the size of emitted particles reduce their number concentration (for a fixed value of FF_Ems). The globally consistent sign of forcing response to parameter perturbations makes fossil fuel emission parameters the dominant sources of global-mean CAE forcing variance, despite making relatively small percentage contributions to regional forcing variance. The decline in importance of fossil fuel emission parameters as sources of global-mean CAE forcing uncertainty when adjusted for the cancellation of positive and negative regional forcings (Fig. 5), suggests that other parameters make far larger regionally important contributions to uncertainty in CAE forcing.

The pattern of contributions to variance for the emission flux of SO_2 aerosols from continuously degassing and sporadically erupting volcanoes (Volc_SO2; Fig. 6b) contrasts with the FF_Diam pattern. Increasing Volc_SO2 in regions where it contributes to CAE forcing variance suppresses the magnitude of both positive and negative forcing, simply because the volcanic aerosol raises the natural background CDNC against which anthropogenic forcing is defined (S5). Volc_SO2 makes its largest contribution to variance in regions of relatively low aerosol concentrations (Schmidt et al. 2012); however, in some regions aerosol concentrations are lowest in 1978 and in other regions in 2008. The cancellation of positive and negative regional forcings in global CAE forcing calculations masks the importance of Volc_SO2 as a source of aerosol forcing uncertainty. The lower importance of this natural emission parameter to the uncertainty in recent decadal forcing (Regayre et al. 2014) versus forcing since the preindustrial era (Carslaw et al. 2013) is mostly related to regional cancellation in the Regayre et al. (2014) study.

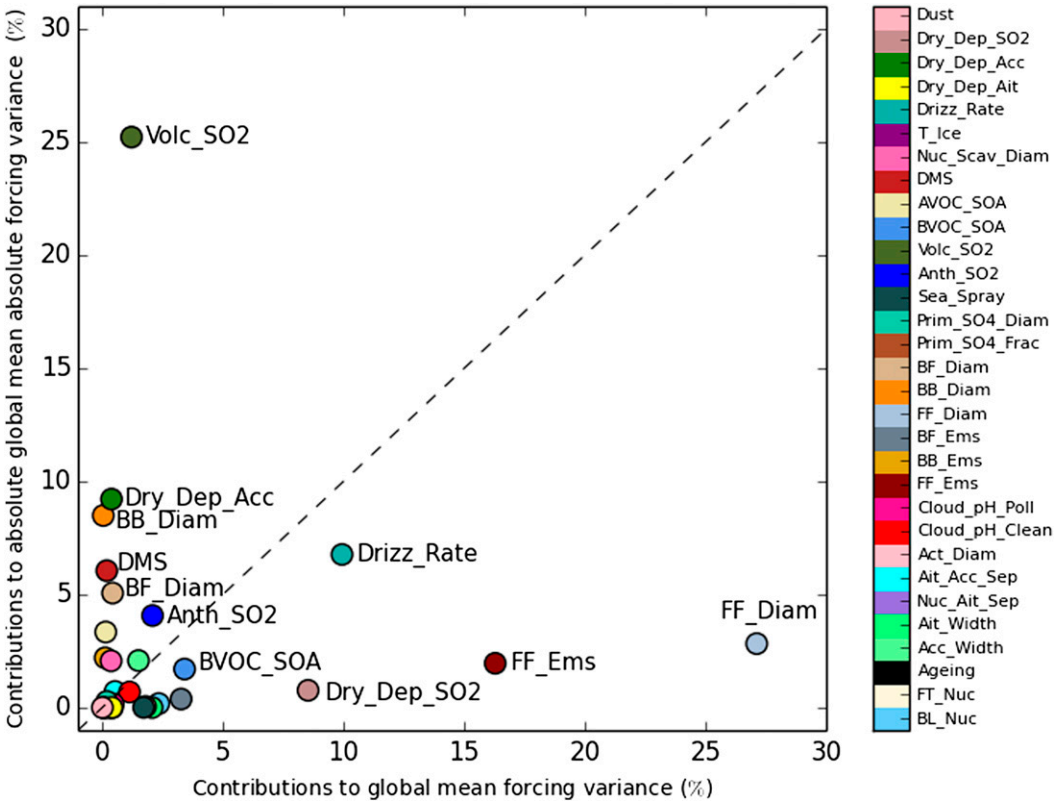

FIG. 5. Global-mean CAE forcing and global-mean absolute CAE forcing percentage contributions to variance for each aerosol parameter. The dashed diagonal line is the 1:1 line.

b. *Regional forcing sensitivities*

A sensitivity analysis that quantifies contributions to CAE forcing variance from aerosol parameters is conducted here for each of the regions identified as being influential on the climate effects outlined in section 2d. Figures 7–9 summarize the mean regional percentage contributions to variance during the 1978–2008 period. Regional-mean forcings and mean 90% CIs (calculated as outlined in section 2b for months where SSTs are

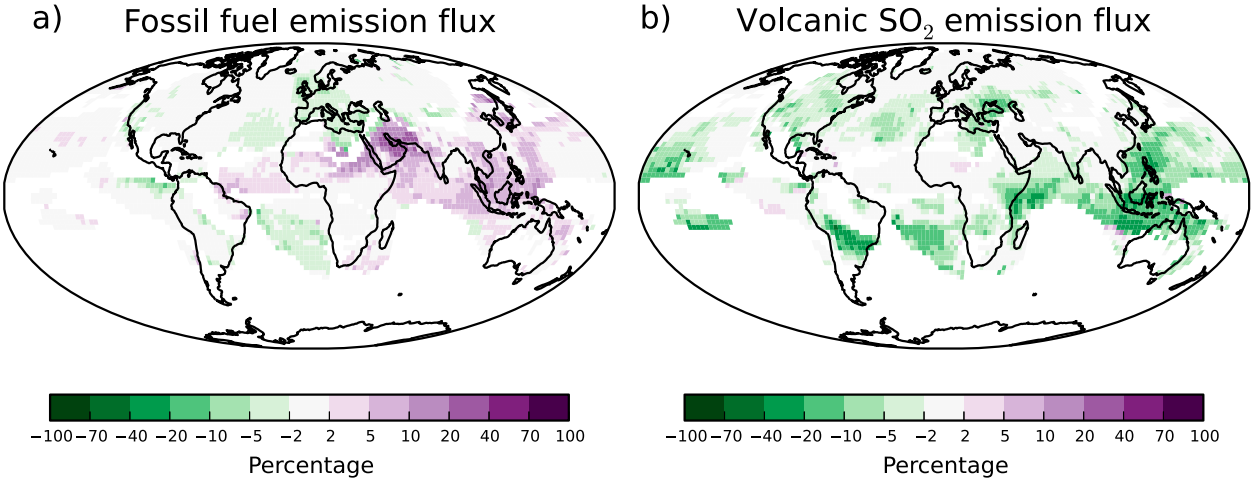

FIG. 6. Percentage contributions to CAE forcing variance for (a) fossil fuel emission flux in May and (b) continuously degassing and sporadically erupting volcanic SO_2 emission flux in June. Purple shading is used to indicate that increasing the parameter amplifies CAE forcing (positive or negative) within individual model grid boxes, and green shading indicates that increasing the parameter suppresses CAE forcing.

climatically important) are summarized in Table 2. While the global-mean simulated CAE forcing is a small fraction of the forcing caused by changes in anthropogenic CO_2 emissions (Regayre et al. 2014), Fig. 10 illustrates that in many climatically important regions the uncertainty in CAE forcing, arising from uncertainty in aerosol emissions and process parameters, is at least as important as forcing arising from changing CO_2 emissions during this period. Very similar spatial response patterns result when the Myhre et al. (2013) global-mean value of $0.7\,W\,m^{-2}$ is used to represent the forcing caused by changes in anthropogenic CO_2 emissions in the ratio calculation.

1) Intertropical convergence zone and Sahel precipitation

A negative mean CAE forcing in the tropical North Atlantic (R2) of $-0.05\,W\,m^{-2}$ contrasts with the positive forcing of $0.25\,W\,m^{-2}$ in the tropical South Atlantic (R3). On their own these results suggest that CAE forcing has exacerbated the interhemispheric differences in SSTs in recent decades. The mean CAE forcing in the extratropical North Atlantic (R1) is $0.51\,W\,m^{-2}$, which is the largest annual-mean forcing of the regions examined here. Sources of CAE forcing uncertainty are examined in each Atlantic region (R1–R3) with regard to their potential influence on uncertainty in ITCZ position and Sahel precipitation.

Uncertainty in CAE forcing is of a similar magnitude in all three regions with credible values ranging from 0.37 to $0.65\,W\,m^{-2}$ in the extratropical North Atlantic, from -0.21 to $0.11\,W\,m^{-2}$ in the tropical North Atlantic and from 0.06 to $0.41\,W\,m^{-2}$ in the tropical South Atlantic. The sign of CAE forcing is uncertain in the tropical North Atlantic because negative forcing in the eastern part of this region competes with positive forcing in the west. Positive CAE forcing in the extratropical North Atlantic and negative CAE forcing in the tropical North Atlantic suggest that there may be less hemispheric consensus in the sign of the forcing resulting from reductions in anthropogenic aerosol emissions than previously appreciated.

In each of the regions where CAE forcing is thought to have an influence on the position of the ITCZ (R2 and R3) and Sahel precipitation (R1–R3), CAE forcing variance is determined by a distinct combination of parameters; however, anthropogenic emission fluxes and aerosol process parameters account for the majority of the variance in each case. In the tropical North Atlantic (R2) the largest CAE forcing uncertainty sources in the Northern Hemisphere summer months (when the mean forcing is negative) are the rate of dry deposition of aerosols in the accumulation mode (Dry_Dep_Acc) and FF_Diam. The rate of dry deposition of SO_2 (Dry_Dep_SO2), anthropogenic SO_2 emissions (Anth_SO2), and the formation of secondary organic aerosols (SOA) from anthropogenic volatile organic compounds (VOCs) (AVOC_SOA) are important sources of CAE forcing uncertainty in the tropical North Atlantic during the months where forcing is negative. These same parameters contribute substantially to CAE forcing variance in the extratropical North Atlantic (R1) for much of the year, suggesting that, during the Northern Hemisphere winter, uncertainty in North American anthropogenic emissions is influential on SST in the tropical North Atlantic.

Contributions to CAE forcing variance in the tropical South Atlantic (R3) are diverse; however, the majority are accounted for by the emitted particle diameter of aerosols from biomass burning sources (BB_Diam), the rate of precipitation scavenging in warm low-level stratocumulus clouds (Drizz_Rate), and Anth_SO2. Uncertainty sources in the tropical South Atlantic are so varied that constraining all aerosol parameters that contribute to CAE forcing variance on decadal time scales is unrealistic. Instead, representations of ITCZ position could be more readily improved by reducing the uncertainty in Drizz_Rate, which is the largest source of uncertainty in October when the mean regional forcing is largest.

2) North Atlantic tropical storm development

Contributions to CAE forcing uncertainty in the extratropical and tropical North Atlantic (R1 and R2) are examined here, as in section 3b(1). Analysis is restricted to the warmest Northern Hemisphere months when tropical storms predominate.

The tropical North Atlantic (R2) has a smaller absolute-mean regional CAE forcing and uncertainty range, between April and October, than the extratropical North Atlantic (R1). Credible values range from -0.33 to $0.02\,W\,m^{-2}$ in the tropical North Atlantic and range from 0.54 to $0.95\,W\,m^{-2}$ in the extratropical North Atlantic. The mean simulated CAE forcing in the tropical North Atlantic (R2) is negative ($-0.14\,W\,m^{-2}$). The positive CAE forcing in the wider North Atlantic (e.g., $0.75\,W\,m^{-2}$ in R1) supports the hypothesis that reductions in Northern Hemispheric aerosol emissions have warmed SSTs and acted as one of the drivers of recent decadal increases in Atlantic tropical storms (Booth et al. 2012). However, the simulated CAE forcing in the tropical North Atlantic ($-0.14\,W\,m^{-2}$), which roughly aligns with the main Atlantic hurricane development region, is of the opposite sign from that suggested by Dunstone et al. (2013) as being consistent with an aerosol driver of tropical storm changes. The

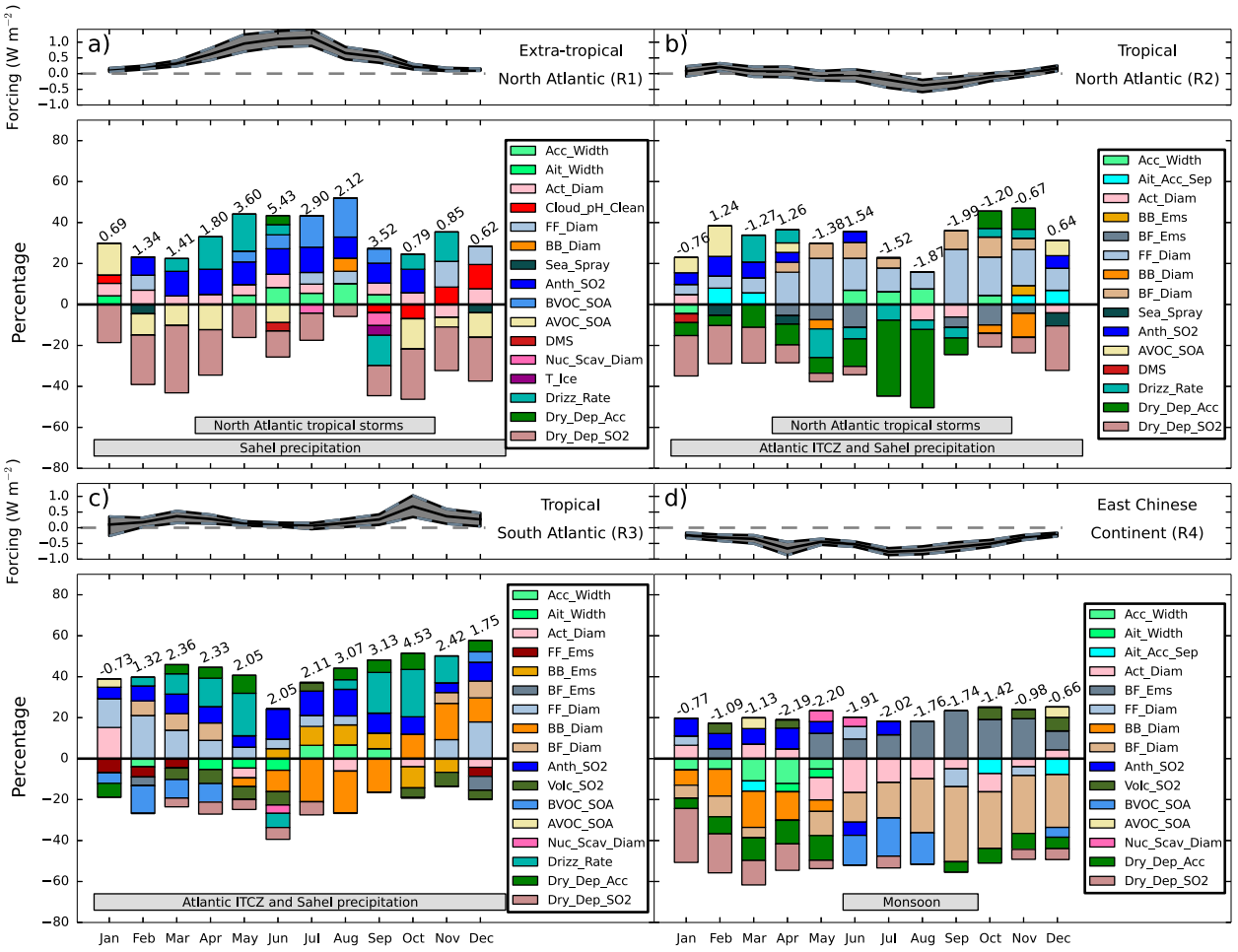

FIG. 7. Regional-mean percentage contributions to CAE forcing variance for R1–R4. Contributions of less than 4% of the CAE forcing variance are omitted. A reminder of climatically important effects is provided using shaded text under the appropriate months. Where increasing a parameter leads to an amplification of positive or negative CAE forcing (S1, S4, and S6 in Fig. 3), the percentage contributions are above the *x* axis. If a parameter increase leads to suppression of CAE forcing in the region (S2, S3, and S5), then the contributions are below the *x* axis. A time series of average forcing values is included in a panel at the top of each plot with mean regional 90% CIs shaded gray. CAE forcing in the model grid box where absolute CAE forcing is strongest is presented above the bar for each month.

credible range of simulated tropical North Atlantic CAE forcing includes positive values. However, unless physical grounds are found for ruling out parameter combinations that lead to mean CAE forcing values in the lower part of this range, these results call into question the relationship between Northern Hemisphere aerosol emission reductions and CAE forcing of SSTs in the main Atlantic hurricane development region on decadal time scales.

In the tropical North Atlantic (R2) Dry_Dep_Acc and FF_Diam contribute most to forcing variance in months relevant to tropical storm development, while Anth_SO2 and Dry_Dep_SO2 contribute most to variance in the extratropical North Atlantic (R1). Uncertainty in tropical storm development in the Atlantic Ocean in recent decades, insofar as it is affected by CAE forcing on SST, is largely determined by uncertainties in aerosol deposition process parameters and anthropogenic emission fluxes.

3) PACIFIC TROPICAL STORM DEVELOPMENT

The northwestern Pacific Ocean (R9) has a simulated-mean CAE forcing of $-0.20\,\mathrm{W\,m^{-2}}$ with credible values ranging from -0.33 to $-0.06\,\mathrm{W\,m^{-2}}$, making the magnitude of its role in Pacific tropical storm development in recent decades highly uncertain. Figure 9a shows that the magnitude and uncertainty in CAE forcing are largest in the Northern Hemisphere summer months when a negative forcing will reduce SSTs and therefore potentially suppress tropical storm development. During January and February when anthropogenic aerosol emissions may alter the Pacific

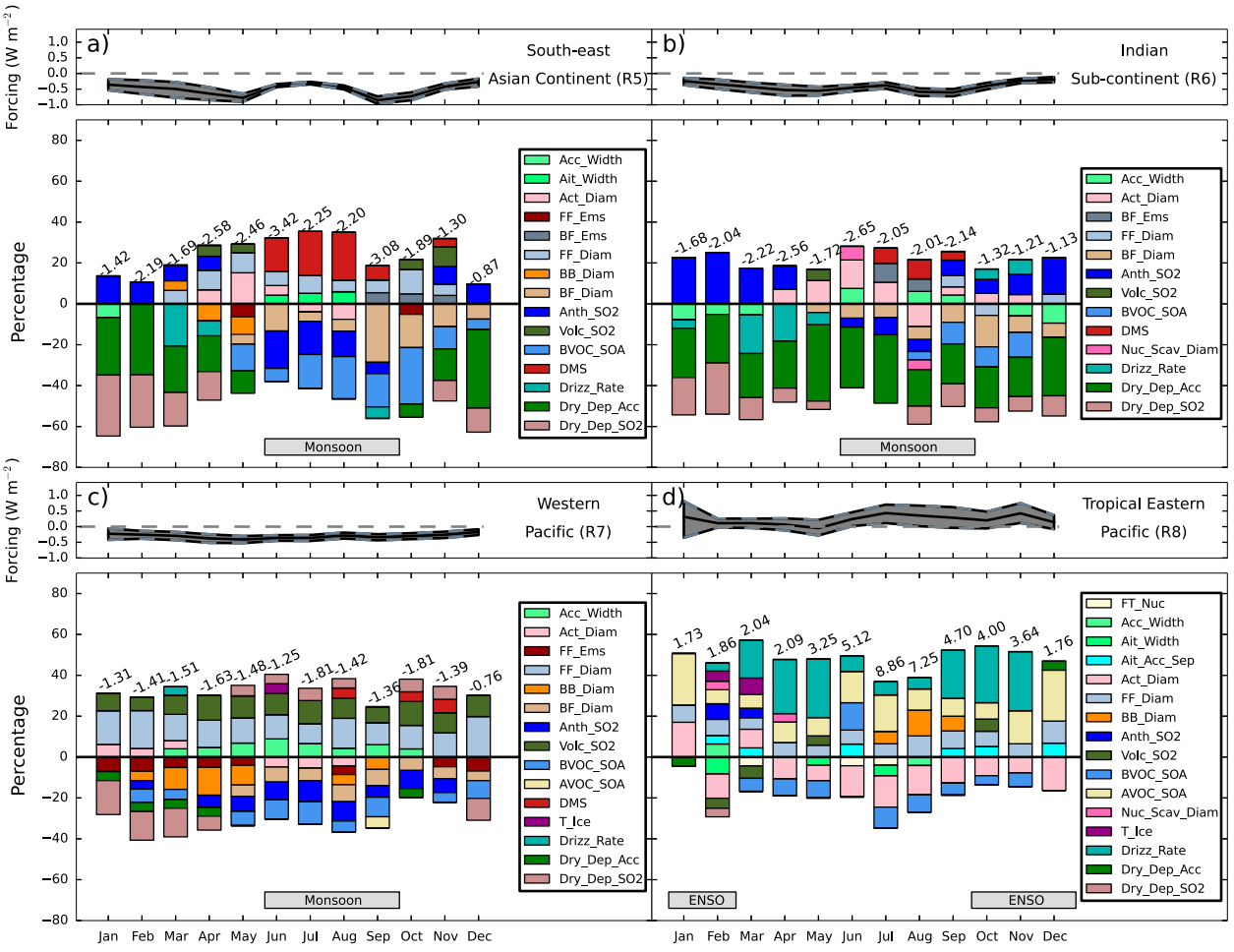

FIG. 8. Regional-mean percentage contributions to CAE forcing variance for R5–R8. Features are identical to Fig. 7.

storm track (Wang et al. 2014a), the magnitude of CAE forcing is near zero with relatively little uncertainty, suggesting that, if anthropogenic aerosol emissions do affect the Pacific storm track, it is through aerosol feedbacks on clouds and meteorology not modeled here.

The sources of CAE forcing uncertainty in the northwestern Pacific (R9) are numerous and temporally dependent. Dry_Dep_SO2 makes the largest contribution to CAE forcing variance during the early months of the year, relevant to the potential influence of aerosols on the Pacific storm track. The sources of CAE forcing uncertainty are diverse during other months, indicating that reducing uncertainty in the role of CAE forcing in Pacific tropical storm development will require a combination of developments in the representation of aerosol emission fluxes and aerosol process parameters.

4) ASIAN SUMMER MONSOON

The gradient in land–sea surface temperatures influences ASM development; hence, the relative magnitudes of CAE forcing in neighboring regions are considered here. Mean CAE forcing between June and September is negative in all regions examined here, and the contrast in forcing is largest between the Chinese continental and marine regions (R4 and R7). The continental CAE forcing is $-0.67\,\mathrm{W\,m^{-2}}$ compared to only $-0.33\,\mathrm{W\,m^{-2}}$ in the neighboring marine region, suggesting that CAE forcing plays an important role in reducing the land–sea thermal contrast. The negative CAE forcing is also stronger in continental Southeast Asia (R5) and India (R6) than in the neighboring Indian Ocean (R10), having respective values of -0.47, -0.51, and $-0.18\,\mathrm{W\,m^{-2}}$. In each of the regions relevant to ASM prediction, the land–sea surface temperature contrast is weakened as a result of CAE forcing, implying CAE forcing contributed to the weakened ASM observed in these regions in recent decades, as outlined in section 2d(3).

Contributions to CAE forcing variance are considered simultaneously for neighboring continental and marine regions in China (R4 and R7), Southeast Asia

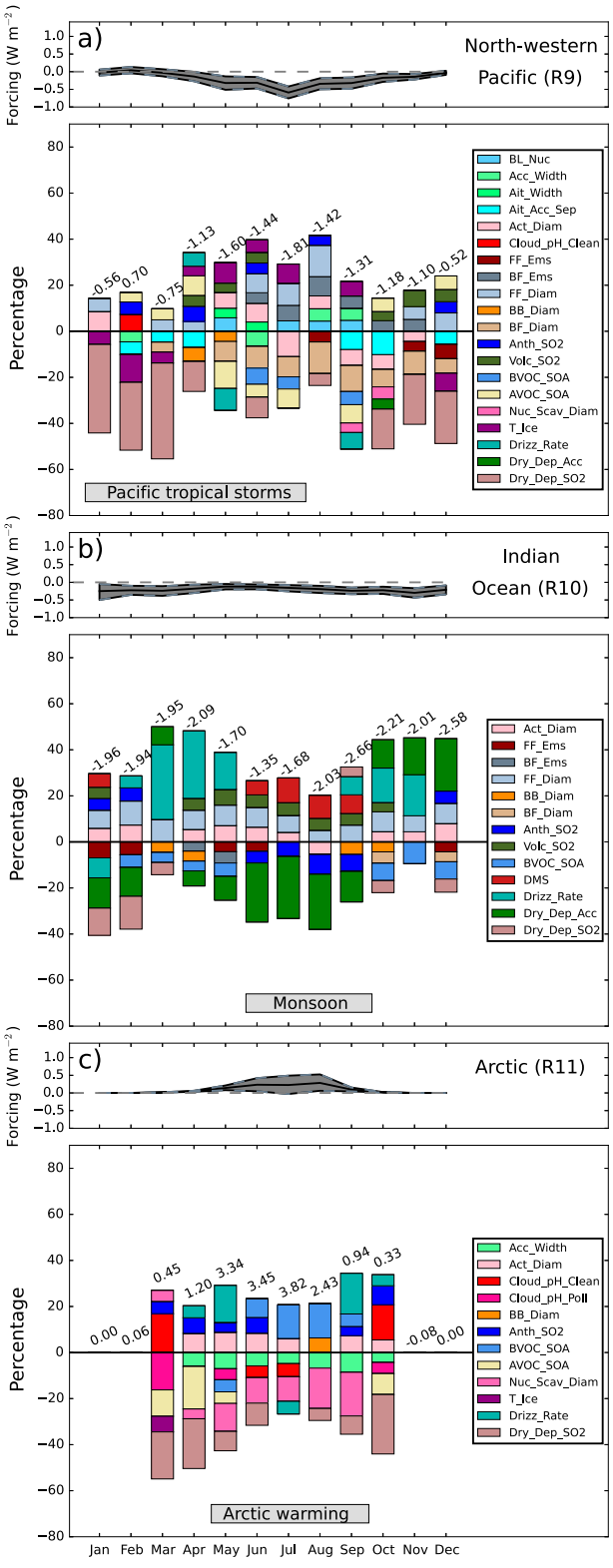

FIG. 9. Regional-mean percentage contributions to CAE forcing variance for R9–R11. Features are identical to Fig. 7.

(R5 and R10), and India (R6 and R10). In continental China (R4) CAE forcing uncertainty is largely determined by biofuel emission flux (BF_Ems) and emitted particle diameter (BF_Diam), and to a lesser extent by SOA formation from biogenic VOCs (BVOC_SOA). In the western Pacific bordering China (R7) FF_Diam, Volc_SO2, and Anth_SO2 make substantial contributions to CAE forcing variance. BVOC_SOA is the only parameter to contribute substantially to uncertainty in CAE forcing in the marine and continental regions.

In Southeast Asia (R5) the largest sources of CAE forcing uncertainty are the emission flux of dimethyl sulfide (DMS), BF_Diam, Anth_SO2, and BVOC_SOA. Many of the important uncertainty sources in Southeast Asia (R5) also contribute to CAE forcing variance in the Indian Ocean (R10). The aerosol removal process parameters Dry_Dep_Acc and Drizz_Rate are the largest sources of CAE forcing uncertainty over the Indian Ocean. Dry_Dep_Acc also makes the largest contribution to CAE forcing variance over the Indian continent (R6), with smaller contributions coming from DMS, BF_Ems, BF_Diam, and the diameter at which aerosols are considered large enough to have the potential to act as cloud condensation nuclei (CCN) (Act_Diam).

The importance of biofuel carbonaceous aerosol parameters BF_Ems and BF_Diam as sources of CAE forcing uncertainty is largely restricted to the continental regions where they are produced. Uncertainty in the magnitude of CAE forcing in the Indian Ocean and Indian continent can be reduced by improving the representation of Dry_Dep_Acc. Anth_SO2 also plays an important role in both continental and marine regions, confirming the results of Verma et al. (2013). Neighboring land and marine regions in Southeast Asia and China are sensitive to noticeably different combinations of aerosol parameters. Wang et al. (2014) show that CMIP5 models typically underestimate CAE forcing in the western Pacific and over China. The aerosol emission fluxes and model processes identified here provide a foundation for examining the cause of CAE forcing underestimation and for reducing the effect of uncertainty in CAE forcing on ASM prediction.

5) El Niño–Southern Oscillation

Changes in SSTs in the tropical eastern Pacific Ocean (R8), where anomalously warm or cold SSTs in the Pacific Ocean typically initially develop, are used to determine changes to the mean state of the ENSO (Rasmusson and Carpenter 1982). The sign of forcing is likely positive in the tropical eastern Pacific with mean CAE forcing of 0.24 W m^{-2} and simulated credible values ranging from −0.08 to 0.53 W m^{-2}. The upper

TABLE 2. Regional-mean CAE forcings and mean 90% CIs for months where CAE forcing influences climatic effects. The largest absolute individual model gridbox mean CAE forcings within each region are provided for the months of interest (indicated in Table 1). Ratios of mean regional CAE forcing 90% credible interval range to the forcing caused by changes in anthropogenic CO_2 emissions, using the months of interest, provide context for the relative importance of regional CAE forcing uncertainties.

Key	Location	Climate effect	Mean forcing ($W\,m^{-2}$)	Mean 90% CI ($W\,m^{-2}$)	Largest absolute-mean forcing ($W\,m^{-2}$)	Ratio of mean forcings (CAE:CO_2)
R1	Extratropical North Atlantic	North Atlantic tropical storms	0.75	(0.54, 0.95)	2.88	0.59
R1	Extratropical North Atlantic	Sahel precipitation	0.51	(0.37, 0.66)	2.09	0.41
R2	Tropical North Atlantic	North Atlantic tropical storms	−0.14	(−0.33, 0.02)	−0.96	0.32
R2	Tropical North Atlantic	Atlantic ITCZ and Sahel precipitation	−0.05	(−0.21, 0.11)	−0.63	0.44
R3	Tropical South Atlantic	Atlantic ITCZ and Sahel precipitation	0.25	(0.06, 0.41)	2.20	0.50
R4	East China	Asian summer monsoon	−0.66	(−0.77, −0.54)	−1.86	0.33
R5	Southeast Asia	Asian summer monsoon	−0.47	(−0.57, −0.43)	−2.74	0.20
R6	Indian subcontinent	Asian summer monsoon	−0.51	(−0.63, −0.40)	−2.22	0.32
R7	Western Pacific	Asian summer monsoon	−0.33	(−0.43, −0.24)	−1.46	0.27
R8	Tropical eastern Pacific	ENSO development	0.24	(−0.08, 0.53)	2.60	0.88
R9	Northwestern Pacific	Pacific tropical storms	−0.20	(−0.33, −0.06)	−0.94	0.38
R10	Indian Ocean	Asian summer monsoon	−0.18	(−0.27, −0.10)	−1.93	0.25
R11	Arctic	Arctic warming	0.20	(0.04, 0.36)	2.80	0.57

credible CAE forcing value indicates that there may have been as much as 1×10^{11} J of energy entering the tropical eastern Pacific between 1978 and 2008 as a result of positive CAE forcing. The positive CAE forcing in the eastern Pacific is consistent with the shift toward conditions more suitable for El Niño events that occurred at the end of the twentieth century (Trenberth and Hoar 1996). This raises the possibility that past aerosol changes may have influenced the mean ENSO state. The likely positive CAE forcing simulated here suggests that it may be possible that apparent multidecadal shifts in the mean ENSO state in the tropical eastern Pacific, resulting from changing SSTs, are the result of a forced aerosol signal.

The dominant sources of uncertainty in the tropical eastern Pacific (R8) are Drizz_Rate, which contributes most to CAE forcing variance in November when mean forcing is largest, and AVOC_SOA, which contributes in the early months of the year when CAE forcing uncertainty is relatively large. Act_Diam and FF_Diam are also important sources of CAE forcing uncertainty. Improving the representation of these aerosol process

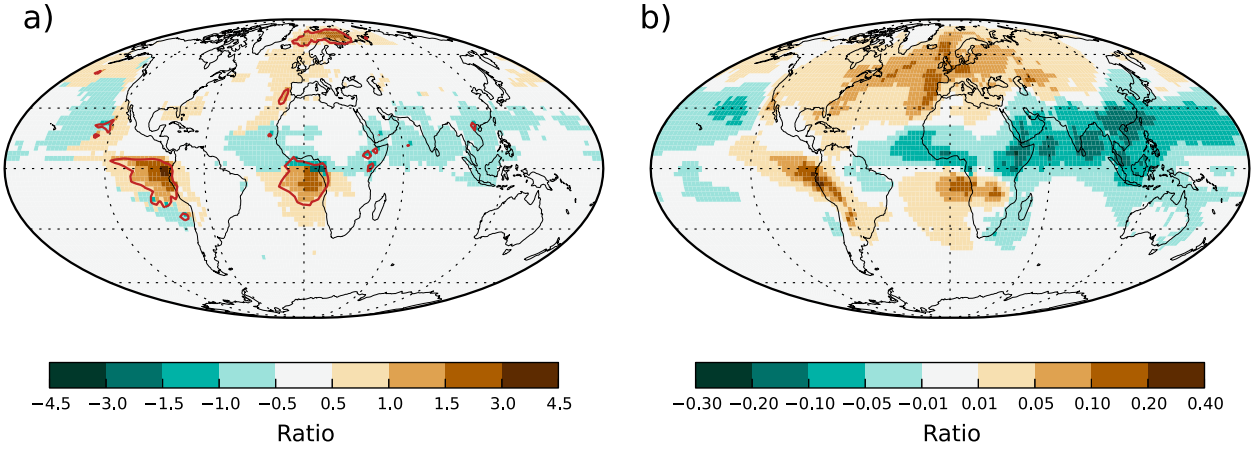

FIG. 10. Regional uncertainty in CAE forcing. (a) Ratio of the annual-mean absolute 90% credible range of CAE forcing to the forcing caused by changes in anthropogenic CO_2 emissions, calculated within individual model grid boxes. The contours indicate locations where the regional CAE forcing credible range and global-mean CO_2 change forcing are equal. Ratios are calculated independently within individual model grid boxes and credible ranges have been multiplied by −1 where global-mean CAE forcing is negative. (b) Ratio of annual-mean CAE forcing to simulated CO_2 induced forcing.

and emission flux parameters will reduce uncertainty in the magnitude of the CAE forcing in recent decades, allowing further research into the potential for an aerosol-forced signal to influence the mean ENSO state on multidecadal time scales conducted with better constrained CAE forcing values.

6) ARCTIC

The sign of CAE forcing in the Arctic (R11) is likely positive with credible values ranging from 0.04 to 0.36 $W m^{-2}$. A positive CAE forcing in the Arctic agrees with the results of Shindell and Faluvegi (2009) and Chylek et al. (2014), which suggest that decreasing North American and European anthropogenic emissions in recent decades have contributed to Arctic warming.

The pH of water within clouds in relatively clean (Cloud_pH_Clean) and polluted (Cloud_pH_Poll) atmospheric environments affects the rate of secondary sulfate formation, and both parameters are important sources of CAE forcing uncertainty in the Arctic, where anthropogenic emissions have often been transported relatively long distances from Northern Hemisphere continental regions (Law et al. 2014). Cloud_pH_Poll contributes more to CAE forcing variance than Cloud_pH_Clean in the Northern Hemisphere summer months when the forcing is strongest.

The important contributions of aerosol process parameters to CAE forcing in the Arctic is indicative that the uncertainties are related to the processing of aerosols during transport into this region. Furthermore, the dominance of aerosol process parameters in this region suggests that multimodel CAE forcing diversity in the Arctic is likely to be larger than in other regions.

4. Conclusions

During the 1978–2008 period, changes in anthropogenic CO_2 emissions cause a global-mean forcing of 0.7 $W m^{-2}$ (Myhre et al. 2013). Regayre et al. (2014) calculated a near-zero global-mean CAE forcing with high confidence during the 1978–2008 period. However, it is shown here that substantial regional aerosol CAE forcing uncertainties of climatic importance exist. The disparity between the magnitudes and degree of uncertainty in global and regional mean CAE forcings is explained by the cancellation of positive and negative regional forcings.

Performing a sensitivity analysis on global-mean absolute CAE forcing has revealed a number of parametric contributions to CAE forcing variance that were not identified in the sensitivity analysis of global CAE forcing conducted by Regayre et al. (2014). Continuously degassing and sporadically erupting volcanic SO_2 emissions, the rate of dry deposition of aerosols in the accumulation mode, and the diameter of carbonaceous aerosols emitted from biomass burning sources all contributed very little to global-mean CAE forcing uncertainty, yet here it is shown that across the globe these parameters are the main sources of uncertainty on the regional scale. The drizzle rate within low-level stratocumulus clouds is an important source of uncertainty for global-mean CAE forcing with and without the cancellation of positive and negative regional forcings. The emission flux and diameter of organic carbon and black carbon aerosols from fossil fuel sources cause most of the uncertainty in global-mean CAE forcing, yet they are relatively small sources of uncertainty in global-mean absolute CAE forcing, each explaining less than 5% of the variance. The large contributions of fossil fuel parameters to global-mean CAE forcing arise because other parameters experience a greater degree of regional forcing cancellation in the global-mean calculation.

Aerosol parameter contributions to regional CAE forcing variance have been analyzed in 11 regions where CAE forcing is believed to influence large-scale climate effects. Within the climatically important regions examined, anthropogenic aerosol emission fluxes and aerosol process parameters are typically the largest sources of CAE forcing uncertainty. However, in many regions there is at least one natural aerosol emission flux that plays an important role. When attempting to constrain regional CAE forcing over recent decades, uncertainties in natural emission fluxes cannot be ignored. In particular the emission flux of SO_2 from continuously degassing and sporadically erupting volcanoes and the formation of SOA from biogenic VOCs contribute a small percentage of CAE forcing variance in almost all regions.

Quantifying the magnitude and uncertainty in regional CAE forcing provides insight into the potential for CAE forcing to influence large-scale climate effects. Our calculated uncertainty ranges leave open the possibility that CAE forcing may act against, rather than drive, the observed reduction in interhemispheric SST gradient in the Atlantic since the late 1970s. Considering the broader North Atlantic, the strong positive CAE forcing in the extratropical North Atlantic may influence ITCZ position and width. A negative CAE forcing in the tropical North Atlantic during recent decades calls into question whether further reductions in Northern Hemisphere anthropogenic aerosol emissions will lead to further increases in Atlantic storminess. CAE forcing is unlikely to be the cause of recent changes in the Pacific storm track although it has the potential to affect SSTs and therefore storm frequency in summer months. Our results support the hypothesis

that the observed changes in the ASM in recent decades are in part driven by CAE forcing that weakens the SAT/SST gradient in China, Southeast Asia, and India. CAE forcing in the eastern Pacific and uncertainty in the forcing are shown here to be substantial, allowing us to speculate that apparent shifts in the mean ENSO state, determined using changes in SST, may result from a forced aerosol signal on multidecadal time scales. Our results also support the hypothesis that CAE forcing was positive in the Arctic in recent decades. Uncertainty in simulated CAE forcing is substantial in the Arctic and therefore so is its role in the observed rapid warming of Arctic surface temperatures.

In the atmosphere, aerosols feed back onto meteorology and clouds; however, our experiment was designed to quantify the effect of uncertain aerosol emission fluxes and process parameters on CAE forcing in isolation. The additional uncertainty arising from the representation of atmospheric physics within global models has the potential to affect regional and global CAE forcing calculations. Fasullo and Trenberth (2012) provide clear evidence that teleconnections and feedbacks must be adequately modeled in order to reduce uncertainty in the simulation of climate effects. Furthermore, using a dynamic ocean, rather than prescribing SSTs, in global climate models can produce markedly different climatic responses to external forcings (Ocko et al. 2014; Andrews et al. 2015). Research into the relative importance of uncertainties in aerosol and atmospheric physics parameterizations as sources of CAE forcing uncertainty using global climate models that include representations of aerosol–cloud meteorology and atmosphere–ocean feedbacks is essential. The sources of aerosol parametric uncertainty identified as globally and regionally important here can be used to inform future research where the reduction of CAE forcing variance is a priority.

Acknowledgments. Data can be made available upon request from the corresponding author. L. A. Regayre is funded by a Doctoral Training Grant from the Natural Environment Research Council (NERC) and a CASE studentship with the Met Office Hadley Centre. B. B. B. Booth was supported by the Joint UK DECC/Defra Met Office Hadley Centre Climate Programme (GA01101). K. S. Carslaw acknowledges funding from the Royal Society Wolfson Award. We acknowledge funding from NERC under AEROS and GASSP Grants NE/G006172/1 and NE/J024252/1. This work made use of the facilities of N8 HPC provided and funded by the N8 consortium and EPSRC (EP/K000225/1). The Met Office Hadley Centre is coordinated by the University of Leeds and the University of Manchester. The authors thank three anonymous reviewers for their constructive comments on this article.

REFERENCES

Allen, R. J., S. C. Sherwood, J. R. Norris, and C. S. Zender, 2012: The equilibrium response to idealized thermal forcings in a comprehensive GCM: Implications for recent tropical expansion. *Atmos. Chem. Phys.,* **12,** 4795–4816, doi:10.5194/acp-12-4795-2012.

——, J. R. Norris, and M. Kovilakam, 2014: Influence of anthropogenic aerosols and the Pacific decadal oscillation on tropical belt width. *Nat. Geosci.,* **7,** 270–274, doi:10.1038/ngeo2091.

Andrews, T., J. M. Gregory, and M. J. Webb, 2015: The dependence of radiative forcing and feedback on evolving patterns of surface temperature change in climate models. *J. Climate,* **28,** 1630–1648, doi:10.1175/JCLI-D-14-00545.1.

Barahona, D., R. E. L. West, P. Stier, S. Romakkaniemi, and A. Nenes, 2010: Comprehensively accounting for the effect of giant CCN in cloud activation parameterizations. *Atmos. Chem. Phys.,* **10,** 2467–2473, doi:10.5194/acp-10-2467-2010.

Bollasina, M. A., Y. Ming, and V. Ramaswamy, 2013: Earlier onset of the Indian monsoon in the late twentieth century: The role of anthropogenic aerosols. *Geophys. Res. Lett.,* **40,** 3715–3720, doi:10.1002/grl.50719.

Boo, K. O., B. B. B. Booth, Y. H. Byun, J. Lee, C. Cho, S. Shim, and K. T. Kim, 2015: Influence of aerosols in multidecadal SST variability simulations over the North Pacific. *J. Geophys. Res. Atmos.,* **120,** 517–531, doi:10.1002/2014JD021933.

Booth, B. B. B., N. J. Dunstone, P. R. Halloran, T. Andrews, and N. Bellouin, 2012: Aerosols implicated as a prime driver of twentieth-century North Atlantic climate variability. *Nature,* **484,** 228–232, doi:10.1038/nature10946.

Boucher, O., and Coauthors, 2013: Clouds and aerosols. *Climate Change 2013: The Physical Science Basis,* T. F. Stocker et al., Eds., Cambridge University Press, 571–657. [Available online at http://www.climatechange2013.org/images/report/WG1AR5_Chapter07_FINAL.pdf.]

Calisto, M., D. Folini, M. Wild, and L. Bengtsson, 2014: Cloud radiative forcing intercomparison between fully coupled CMIP5 models and CERES satellite data. *Ann. Geophys.,* **32,** 793–807, doi:10.5194/angeo-32-793-2014.

Carslaw, K. S., and Coauthors, 2013: Large contribution of natural aerosols to uncertainty in indirect forcing. *Nature,* **503,** 67–71, doi:10.1038/nature12674.

Chang, C. Y., J. C. H. Chiang, M. F. Wehner, A. Friedman, and R. Ruedy, 2011: Sulfate aerosol control of tropical Atlantic climate over the twentieth century. *J. Climate,* **24,** 2540–2555, doi:10.1175/2010JCLI4065.1.

Chiang, J. C. H., C. Y. Chang, and M. F. Wehner, 2013: Long-term behavior of the Atlantic interhemispheric SST gradient in the CMIP5 historical simulations. *J. Climate,* **26,** 8628–8640, doi:10.1175/JCLI-D-12-00487.1.

Choi, J., S. W. Son, J. Lu, and S. K. Min, 2014: Further observational evidence of Hadley cell widening in the Southern Hemisphere. *Geophys. Res. Lett.,* **41,** 2590–2597, doi:10.1002/2014GL059426.

Chylek, P., N. Hengartner, G. Lesins, J. D. Klett, O. Humlum, M. Wyatt, and M. Dubey, 2014: Isolating the anthropogenic component of Arctic warming. *Geophys. Res. Lett.,* **41,** 3569–3576, doi:10.1002/2014GL060184.

Cvijanovic, I., and J. C. Chiang, 2013: Global energy budget changes to high latitude North Atlantic cooling and the tropical ITCZ response. *Climate Dyn.,* **40,** 1435–1452, doi:10.1007/s00382-012-1482-1.

Diaz, H. F., M. P. Hoerling, and J. K. Eischeid, 2001: ENSO variability, teleconnections and climate change. *Int. J. Climatol.,* **21,** 1845–1862, doi:10.1002/joc.631.

Ding, Y., Z. Wang, and Y. Sun, 2008: Inter-decadal variation of the summer precipitation in east China and its association with decreasing Asian summer monsoon. Part I: Observed evidences. *Int. J. Climatol.,* **28,** 1139–1161, doi:10.1002/joc.1615.

Dong, L., and T. Zhou, 2014: The Indian Ocean sea surface temperature warming simulated by CMIP5 models during the twentieth century: Competing forcing roles of GHGs and anthropogenic aerosols. *J. Climate,* **27,** 3348–3362, doi:10.1175/JCLI-D-13-00396.1.

Dunstone, N. J., D. M. Smith, B. B. B. Booth, L. Hermanson, and R. Eade, 2013: Anthropogenic aerosol forcing of Atlantic tropical storms. *Nat. Geosci.,* **6,** 534–539, doi:10.1038/ngeo1854.

Edwards, J. M., and A. Slingo, 1996: Studies with a flexible new radiation code. I: Choosing a configuration for a large-scale model. *Quart. J. Roy. Meteor. Soc.,* **122,** 689–719, doi:10.1002/qj.49712253107.

Evan, A. T., D. J. Vimont, A. K. Heidinger, J. P. Kossin, and R. Bennartz, 2009: The role of aerosols in the evolution of tropical North Atlantic Ocean temperature anomalies. *Science,* **324,** 778–781, doi:10.1126/science.1167404.

Fadnavis, S., K. Semeniuk, L. Pozzoli, M. G. Schultz, S. D. Ghude, S. Das, and R. Kakatkar, 2013: Transport of aerosols into the UTLS and their impact on the Asian monsoon region as seen in a global model simulation. *Atmos. Chem. Phys.,* **13,** 8771–8786, doi:10.5194/acp-13-8771-2013.

Fasullo, J. T., and K. E. Trenberth, 2012: A less cloudy future: The role of subtropical subsidence in climate sensitivity. *Science,* **338,** 792–794, doi:10.1126/science.1227465.

Folland, C. K., T. N. Palmer, and D. E. Parker, 1986: Sahel rainfall and worldwide sea temperatures, 1901–85. *Nature,* **320,** 602–607, doi:10.1038/320602a0.

Fountoukis, C., and A. Nenes, 2005: Continued development of a cloud droplet formation parameterization for global climate models. *J. Geophys. Res.,* **110,** D11212, doi:10.1029/2004JD005591.

Friedman, A. R., Y. T. Hwang, J. C. H. Chiang, and D. M. W. Frierson, 2013: Interhemispheric temperature asymmetry over the twentieth century and in future projections. *J. Climate,* **26,** 5419–5433, doi:10.1175/JCLI-D-12-00525.1.

Gillett, N. P., D. A. Stone, P. A. Stott, T. Nozawa, A. Yu. Karpechko, G. C. Hegerl, M. F. Wehner, and P. D. Jones, 2008: Attribution of polar warming to human influence. *Nat. Geosci.,* **1,** 750–754, doi:10.1038/ngeo338.

Gong, D. Y., and C. H. Ho, 2003: Arctic oscillation signals in the East Asian summer monsoon. *J. Geophys. Res.,* **108,** 4066, doi:10.1029/2002JD002193.

Granier, C., and Coauthors, 2011: Evolution of anthropogenic and biomass burning emissions of air pollutants at global and regional scales during the 1980–2010 period. *Climatic Change,* **109,** 163–190, doi:10.1007/s10584-011-0154-1.

Guo, L., E. J. Highwood, L. C. Shaffrey, and A. G. Turner, 2013: The effect of regional changes in anthropogenic aerosols on rainfall of the East Asian summer monsoon. *Atmos. Chem. Phys.,* **13,** 1521–1534, doi:10.5194/acp-13-1521-2013.

Hamilton, D. S., L. A. Lee, K. J. Pringle, C. L. Reddington, D. V. Spracklen, and K. S. Carslaw, 2014: Occurrence of pristine aerosol environments on a polluted planet. *Proc. Natl. Acad. Sci. USA,* **111,** 18 466–18 471, doi:10.1073/pnas.1415440111.

Henriksson, S. V., and Coauthors, 2014: Spatial distributions and seasonal cycles of aerosol climate effects in India seen in a global climate–aerosol model. *Atmos. Chem. Phys.,* **14,** 10 177–10 192, doi:10.5194/acp-14-10177-2014.

Hermanson, L., and R. T. Sutton, 2010: Case studies in interannual to decadal climate predictability. *Climate Dyn.,* **35,** 1169–1189, doi:10.1007/s00382-009-0672-y.

Hwang, Y. T., D. M. W. Frierson, and S. M. Kang, 2013: Anthropogenic sulfate aerosol and the southward shift of tropical precipitation in the late 20th century. *Geophys. Res. Lett.,* **40,** 2845–2850, doi:10.1002/grl.50502.

IPCC, 2013: Summary for policymakers. *Climate Change 2013: The Physical Science Basis,* T. F. Stocker et al., Eds., Cambridge University Press, 1–29. [Available online at https://www.ipcc.ch/pdf/assessment-report/ar5/wg1/WGIAR5_SPM_brochure_en.pdf.]

Kang, S. M., and J. Lu, 2012: Expansion of the Hadley cell under global warming: Winter versus summer. *J. Climate,* **25,** 8387–8393, doi:10.1175/JCLI-D-12-00323.1.

Kirtman, B., and Coauthors, 2013: Near-term climate change: Projections and predictability. *Climate Change 2013: The Physical Science Basis,* T. F. Stocker et al., Eds., Cambridge University Press, 953–1028. [Available online at https://www.ipcc.ch/pdf/assessment-report/ar5/wg1/WG1AR5_Chapter11_FINAL.pdf.]

Lamarque, J. F., and Coauthors, 2010: Historical (1850–2000) gridded anthropogenic and biomass burning emissions of reactive gases and aerosols: Methodology and application. *Atmos. Chem. Phys.,* **10,** 7017–7039, doi:10.5194/acp-10-7017-2010.

Law, K. S., and Coauthors, 2014: Arctic air pollution: New insights from POLARCAT-IPY. *Bull. Amer. Meteor. Soc.,* **95,** 1873–1895, doi:10.1175/BAMS-D-13-00017.1.

Lee, L. A., K. S. Carslaw, K. J. Pringle, G. W. Mann, and D. V. Spracklen, 2011: Emulation of a complex global aerosol model to quantify sensitivity to uncertain parameters. *Atmos. Chem. Phys.,* **11,** 12 253–12 273, doi:10.5194/acp-11-12253-2011.

——, ——, ——, and ——, 2012: Mapping the uncertainty in global CCN using emulation. *Atmos. Chem. Phys.,* **12,** 9739–9751, doi:10.5194/acp-12-9739-2012.

——, K. J. Pringle, C. L. Reddington, G. W. Mann, P. Stier, D. V. Spracklen, J. Pierce, and K. S. Carslaw, 2013: The magnitude and causes of uncertainty in global model simulations of cloud condensation nuclei. *Atmos. Chem. Phys.,* **13,** 8879–8914, doi:10.5194/acp-13-8879-2013.

Li, J., W. C. Wang, Z. Sun, G. Wu, H. Liao, and Y. Liu, 2014: Decadal variation of East Asian radiative forcing due to anthropogenic aerosols during 1850–2100, and the role of atmospheric moisture. *Climate Res.,* **61,** 241–257, doi:10.3354/cr01236.

Li, Z., and Coauthors, 2011: East Asian Studies of Tropospheric Aerosols and their Impact on Regional Climate (EAST-AIRC): An overview. *J. Geophys. Res.,* **116,** D00K34, doi:10.1029/2010JD015257.

Liu, Y., J. C. H. Chiang, C. Chou, and C. M. Patricola, 2014: Atmospheric teleconnection mechanisms of extratropical North Atlantic SST influence on Sahel rainfall. *Climate Dyn.,* **43,** 2797–2811, doi:10.1007/s00382-014-2094-8.

Lu, J., G. A. Vecchi, and T. Reichler, 2007: Expansion of the Hadley cell under global warming. *Geophys. Res. Lett.,* **34,** L06805, doi:10.1029/2006GL028443.

Mann, G. W., K. S. Carslaw, D. V. Spracklen, D. A. Ridley, P. T. Manktelow, M. P. Chipperfield, S. J. Pickering, and C. E. Johnson, 2010: Description and evaluation of GLOMAP-mode: A modal global aerosol microphysics model for the UKCA composition-climate model. *Geosci. Model Dev.,* **3,** 519–551, doi:10.5194/gmd-3-519-2010.

——, and Coauthors, 2012: Intercomparison of modal and sectional aerosol microphysics representations within the same 3-D global chemical transport model. *Atmos. Chem. Phys.,* **12,** 4449–4476, doi:10.5194/acp-12-4449-2012.

Mann, M. E., and K. A. Emanuel, 2006: Atlantic hurricane trends linked to climate change. *Eos, Trans. Amer. Geophys. Union,* **87,** 233–241, doi:10.1029/2006EO240001.

Mao, K. B., Y. Ma, L. Xia, W. Y. Chen, X. Y. Shen, T. J. He, and T. R. Xu, 2014: Global aerosol change in the last decade: An analysis based on MODIS data. *Atmos. Environ.,* **94,** 680–686, doi:10.1016/j.atmosenv.2014.04.053.

McPhaden, M. J., S. E. Zeibak, and H. M. Glantz, 2006: ENSO as an integrating concept in earth science. *Science,* **314,** 1740–1745, doi:10.1126/science.1132588.

Mulitza, S., and Coauthors, 2008: Sahel megadroughts triggered by glacial slowdowns of Atlantic meridional overturning. *Paleoceanography,* **23,** PA4206, doi:10.1029/2008PA001637.

Myhre, G., and Coauthors, 2013: Anthropogenic and natural radiative forcing. *Climate Change 2013: The Physical Science Basis,* T. F. Stocker et al., Eds., Cambridge University Press, 659–740. [Available online at https://www.ipcc.ch/pdf/assessment-report/ar5/wg1/WG1AR5_Chapter08_FINAL.pdf.]

Ocko, I. B., V. Ramaswamy, and Y. Ming, 2014: Contrasting climate responses to the scattering and absorbing features of anthropogenic aerosol forcings. *J. Climate,* **27,** 5329–5345, doi:10.1175/JCLI-D-13-00401.1.

O'Hagan, A., 2006: Bayesian analysis of computer code outputs: A tutorial. *Reliab. Eng. Syst. Saf.,* **91,** 1290–1300, doi:10.1016/j.ress.2005.11.025.

Pielke, R. A, J. Gratz, C. W. Landsea, D. Collins, M. A. Saunders, and R. Musulin, 2008: Normalized hurricane damage in the United States: 1900–2005. *Nat. Hazards Rev.,* **9,** 29–42, doi:10.1061/(ASCE)1527-6988(2008)9:1(29).

Rasmusson, E. M., and T. H. Carpenter, 1982: Variations in tropical sea surface temperature and surface wind fields associated with the Southern Oscillation/El Niño. *Mon. Wea. Rev.,* **110,** 354–384, doi:10.1175/1520-0493(1982)110<0354:VITSST>2.0.CO;2.

Regayre, L. A., and Coauthors, 2014: Uncertainty in the magnitude of aerosol-cloud radiative forcing over recent decades. *Geophys. Res. Lett.,* **41,** 9040–9049, doi:10.1002/2014GL062029.

Robson, J., R. Sutton, and D. Smith, 2013: Predictable climate impacts of the decadal changes in the ocean in the 1990s. *J. Climate,* **26,** 6329–6339, doi:10.1175/JCLI-D-12-00827.1.

Roe, G. H., N. Feldl, K. C. Armour, Y. T. Hwang, and D. M. W. Frierson, 2015: The remote impacts of climate feedbacks on regional climate predictability. *Nat. Geosci.,* **8,** 135–139, doi:10.1038/ngeo2346.

Rossow, W. B., and R. A. Schiffer, 1999: Advances in understanding clouds from ISCCP. *Bull. Amer. Meteor. Soc.,* **80,** 2261–2287, doi:10.1175/1520-0477(1999)080<2261:AIUCFI>2.0.CO;2.

Rotstayn, L. D., and U. Lohmann, 2002: Tropical rainfall trends and the indirect aerosol effect. *J. Climate,* **15,** 2103–2116, doi:10.1175/1520-0442(2002)015<2103:TRTATI>2.0.CO;2.

Saltelli, A., S. Tarantola, and K. P. S. Chan, 1999: A quantitative model-independent method for global sensitivity analysis of model output. *Technometrics,* **41,** 39–56, doi:10.1080/00401706.1999.10485594.

——, K. Chan, and E. M. Scott, 2000: *Sensitivity Analysis.* Wiley, 504 pp.

Salzmann, M., H. Weser, and R. Cherian, 2014: Robust response of Asian summer monsoon to anthropogenic aerosols in CMIP5 models. *J. Geophys. Res. Atmos.,* **119,** 11 321–11 337, doi:10.1002/2014JD021783.

Schmidt, A., K. S. Carslaw, G. W. Mann, A. Rap, K. J. Pringle, D. V. Spracklen, M. Wilson, and P. M. Forster, 2012: Importance of tropospheric volcanic aerosol for indirect radiative forcing of climate. *Atmos. Chem. Phys.,* **12,** 7321–7339, doi:10.5194/acp-12-7321-2012.

Screen, J. A., and I. Simmonds, 2010: The central role of diminishing sea ice in recent Arctic temperature amplification. *Nature,* **464,** 1334–1337, doi:10.1038/nature09051.

Seidel, D. J., F. Qiang, W. J. Randel, and T. J. Reichler, 2008: Widening of the tropical belt in a changing climate. *Nat. Geosci.,* **1,** 21–24, doi:10.1038/ngeo.2007.38.

Serreze, M. C., A. P. Barrett, J. C. Stroeve, D. N. Kindig, and M. M. Holland, 2009: The emergence of surface-based Arctic amplification. *Cryosphere,* **3,** 11–19.

Shanahan, T. M., and Coauthors, 2009: Atlantic forcing of persistent drought in West Africa. *Science,* **324,** 377–380, doi:10.1126/science.1166352.

Shindell, D., and G. Faluvegi, 2009: Climate response to regional radiative forcing during the twentieth century. *Nat. Geosci.,* **2,** 294–300, doi:10.1038/ngeo473.

——, and Coauthors, 2013: Radiative forcing in the ACCMIP historical and future climate simulations. *Atmos. Chem. Phys.,* **13,** 2939–2974, doi:10.5194/acp-13-2939-2013.

Skeie, R. B., T. K. Berntsen, G. Myhre, K. Tanaka, M. M. Kvalevåg, and C. R. Hoyle, 2011: Anthropogenic radiative forcing time series from pre-industrial times until 2010. *Atmos. Chem. Phys.,* **11,** 11 827–11 857, doi:10.5194/acp-11-11827-2011.

Smith, S. J., J. van Aardenne, Z. Klimont, R. J. Andres, A. Volke, and S. D. Arias, 2011: Anthropogenic sulfur dioxide emissions: 1850–2005. *Atmos. Chem. Phys.,* **11,** 1101–1116, doi:10.5194/acp-11-1101-2011.

Spracklen, D. V., K. J. Pringle, K. S. Carslaw, M. P. Chipperfield, and G. W. Mann, 2005: A global off-line model of size-resolved aerosol microphysics: I. Model development and prediction of aerosol properties. *Atmos. Chem. Phys.,* **5,** 2227–2252, doi:10.5194/acp-5-2227-2005.

Stockwell, D. Z., and M. P. Chipperfield, 1999: A tropospheric chemical-transport model: Development and validation of the model transport schemes. *Quart. J. Roy. Meteor. Soc.,* **125,** 1747–1783, doi:10.1002/qj.49712555714.

Taylor, K. E., R. J. Stouffer, and G. A. Meehl, 2012: An overview of CMIP5 and the experiment design. *Bull. Amer. Meteor. Soc.,* **93,** 485–498, doi:10.1175/BAMS-D-11-00094.1.

Trenberth, K. E., and T. J. Hoar, 1996: The 1990–1995 El Niño-Southern Oscillation event: Longest on record. *Geophys. Res. Lett.,* **23,** 57–60, doi:10.1029/95GL03602.

——, and D. J. Shea, 2006: Atlantic hurricanes and natural variability in 2005. *Geophys. Res. Lett.,* **33,** L12704, doi:10.1029/2006GL026894.

Twomey, S., 1977: Influence of pollution on shortwave albedo of clouds. *J. Atmos. Sci.,* **34,** 1149–1152, doi:10.1175/1520-0469(1977)034<1149:TIOPOT>2.0.CO;2.

Verma, S., O. Boucher, H. C. Upadhyaya, and O. Sharma, 2013: Variations in sulphate aerosols concentration during winter

monsoon season for two consecutive years using a general circulation model. *Atmósfera,* **26,** 359–367.

Villarini, G., and G. A. Vecchi, 2013: Projected increases in North Atlantic tropical cyclone intensity from CMIP5 models. *J. Climate,* **26,** 3231–3240, doi:10.1175/JCLI-D-12-00441.1.

Wang, F., S. Yang, and T. Wu, 2014: Radiation budget biases in AMIP5 models over the East Asian monsoon region. *J. Geophys. Res. Atmos.,* **119,** 13 400–13 426, doi:10.1002/2014JD022243.

Wang, T., H. J. Wang, O. H. Otterå, Y. Q. Gao, L. L. Suo, T. Furevik, and L. Yu, 2013: Anthropogenic agent implicated as a prime driver of shift in precipitation in eastern China in the late 1970s. *Atmos. Chem. Phys.,* **13,** 12 433–12 450, doi:10.5194/acp-13-12433-2013.

Wang, Y., R. Zhang, and R. Saravanan, 2014a: Asian pollution climatically modulates mid-latitude cyclones following hierarchical modelling and observational analysis. *Nat. Commun.,* **5,** 3098, doi:10.1038/ncomms4098.

——, and Coauthors, 2014b: Assessing the effects of anthropogenic aerosols on Pacific storm track using a multiscale global climate model. *Proc. Natl. Acad. Sci. USA,* **111,** 6894–6899, doi:10.1073/pnas.1403364111.

Webster, P. J., 1987: The elementary monsoon. *Monsoons,* J. S. Fein and P. L. Stephens, Eds., Wiley, 3–32.

Ye, J., W. Li, L. Li, and F. Zhang, 2013: ''North drying and south wetting'' summer precipitation trend over China and its potential linkage with aerosol loading. *Atmos. Res.,* **125–126,** 12–19, doi:10.1016/j.atmosres.2013.01.007.

Yeh, S. W., W. M. Kim, Y. H. Kim, B. K. Moon, R. J. Park, and C. K. Song, 2013: Changes in the variability of the North Pacific sea surface temperature caused by direct sulfate aerosol forcing in China in a coupled general circulation model. *J. Geophys. Res. Atmos.,* **118,** 1261–1270, doi:10.1029/2012JD017947.

Yun, K. S., J. Y. Lee, and K. J. Ha, 2014: Recent intensification of the South and East Asian monsoon contrast associated with an increase in the zonal tropical SST gradient. *J. Geophys. Res. Atmos.,* **119,** 8104–8116, doi:10.1002/2014JD021692.

Zhang, R., and Coauthors, 2013: Have aerosols caused the observed Atlantic multidecadal variability? *J. Atmos. Sci.,* **70,** 1135–1144, doi:10.1175/JAS-D-12-0331.1.

Zhang, X., F. W. Zwiers, G. C. Hegerl, F. H. Lambert, N. P. Gillett, S. Solomon, P. A. Stott, and T. Nozawa, 2007: Detection of human influence on twentieth-century precipitation trends. *Nature,* **448,** 461–465, doi:10.1038/nature06025.

Zhao, M., and I. M. Held, 2012: TC-permitting GCM simulations of hurricane frequency response to sea surface temperature anomalies projected for the late-twenty-first century. *J. Climate,* **25,** 2995–3009, doi:10.1175/JCLI-D-11-00313.1.